Development of automated mobile marking robot system for free access floor

Takehiro Tsuruta, Kazuyuki Miura and Mikita Miyaguchi

Research and development institute, Takenaka corporation, Japan
E-mail: tsuruta.takehiro@takenaka.co.jp, miura.kauyuki@takenaka.co.jp, mikita.miyaguchi@takenaka.co.jp

Abstract –

Improvement of productivity in construction work is strongly required because a shortage of construction workers has become a major social issue in Japan. Marking work for installing building materials is indispensable. This work is currently carried out manually. If this work can be automated, construction workers can concentrate on installing the building materials. Therefore we intend to improve productivity by automating this work with a mobile marking robot system.

For the first step, we developed the marking robot system for a free access floor. To build this, grid-pattern lines should be drawn on the floor. Our system can automatically mark the intersections of the lines which are the positions for installing pedestal bases of the free access floor. Our system consists of a mobile marking robot and a laser positioning unit. The former is a mobile robot which has the marking device at its center. Cross marks are drawn on the floor by controlling the marking device. The laser unit accurately directs the point and line laser in the target direction and measures the distance to the object on which the laser spot is projected. The marking robot tracks the line laser and arrives at the target area. The deviation between the target position and the robot center is calculated, and the cross mark is drawn exactly on the target position.

This paper describes the mechanism of our system. It also shows the satisfactory tracking performance and marking accuracy in several experiments.

Keywords –

Marking; Mobile robot; Omnidirectional vehicle; Tracking; Free access floor

1 Introduction

A shortage of construction workers has become a major social issue in Japan. In 2015, the number of construction workers was about 73% of what it had been at its peak in 1997. In the construction process, marking work is indispensable. Construction workers need to draw marks and lines on the floors, walls, ceilings, and so on in the construction site in order to install building materials. In recent years, survey technology has progressed remarkably. Instruments such as laser scanners and total stations have been used in construction fields. Some 3D measuring and marking systems using a total station have been reported [1-3]. These systems are not aimed at automating marking work but at increasing the efficiency of manual marking work. By automating this work with mobile marking robots, construction workers will be able to concentrate on installing building materials and productivity will increase. There have been some studies on automated mobile marking robots. The system reported by Tanaka et al. draws specified figures on the ceiling board [4]. This robot needs to detect the edges of three existing pillars in the construction site by using a laser range finder (LRF). If the distance from the robot to pillar is far or the pillar is covered with fire resistant material, this system cannot mark with high accuracy. In the system reported by Zulkifli et al. [5], a camera needs to be installed on the ceiling and calibrated depending on the installation position, which is very laborious and costly work. Moreover, the area in which a robot can mark is limited by the visual field of the camera. Inoue et al. reported a system using a total station and LRF to measure the robot position [6,7]. In this system, the attitude angle of the mobile robot cannot be measured while moving. Therefore, in our viewpoint, it is difficult to stably navigate the mobile robot to the target position. The navigation method from a mark point to another mark point has not been reported in detail. “Laybot” developed by DPR construction [8] can mark lines on slabs for drywall layout. Since it draws lines while running, it is difficult to draw highly precise straight lines.

As a first step, we intended to automate the marking work for installing a free access floor. In order to build the free access floor correctly, grid-pattern lines should be drawn on the floor before they are installed. The intersections of the lines are the positions for installing the pedestal base of the free access floor. This paper deals with the development of the marking robot for automatically drawing cross marks on the floor which indicate the positions for installing the pedestal bases.

The marking robot is guided to the target position by the laser marker. The three dimensional measuring instrument measures the robot position accurately. Based on the actual robot position, the marking pen installed on the robot is controlled and draws the cross mark at the target position. After that, the robot moves to the next target position and continues this cycle. Since this process is fully automated, just giving all the target positions coordinates in advance to this system allows, all the cross marks corresponding to the positions for installing the pedestal bases to be drawn.

2 Outline of the marking robot system

Our system is composed of a laser positioning unit (LPU) and a marking robot (MR). The operation of the marking system is shown in Figure 1. In this figure, r is the distance from the LPU to the screen placed on the MR base and θ is the direction angle of the point laser. In our system, the marking flow is divided into the MR guidance phase and the cross-mark drawing phase.

In the MR guidance phase, the MR travels from the current position, A (r_a,θ), to the next target position B (r_{tgt},θ_{tgt}). At first, the LPU precisely directs the point laser parallel to the floor in the direction of the target position. Secondly the LPU turns the line laser toward the angle θ_{tgt}. The MR base includes cameras and screens. The cameras capture the screen image where the laser spot and line are projected. The MR tracks the moving laser line and travels on the circumference of a circle whose radius is r_a while keeping the screen perpendicular to the line laser. When the angle of the line laser reaches θ_{tgt}, the LPU stops turning the line laser and the MR stops. Subsequently the MR moves backward or forward on the straight line connecting the LPU and the position B so as to approach the target position B while keeping the screen perpendicular to the line laser. The MR stops when the difference between the distance r measured by the LPU and the target distance r_{tgt} become less than the threshold. However the arrival position of the MR does not exactly correspond to the target position. The actual center position of the MR is measured by the LPU and the camera.

In the cross-mark drawing phase, the MR draws a cross mark exactly on the target position. The MR has a marking device which can move a marking pen in the x, y, and vertical directions. The movement value of the marking pen is calculated by comparing the target position B and the actual center position of the MR. By controlling the marking device based on the calculated movement value, a cross mark whose center corresponds to the target position B is drawn on the floor.

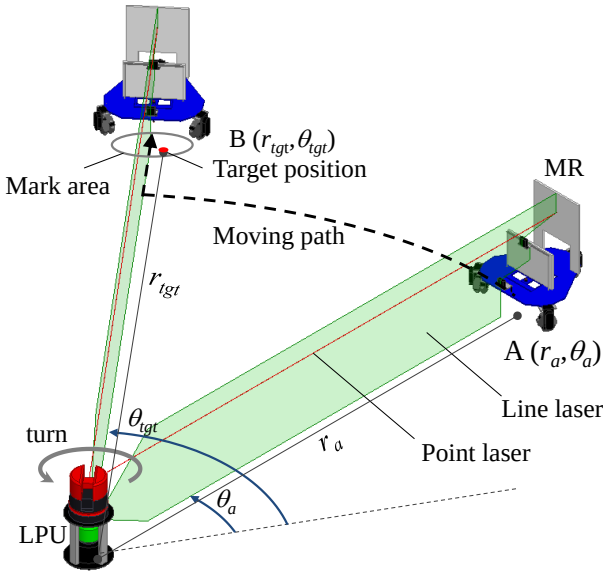

Figure 1. Outline of the marking flow using marking robot system

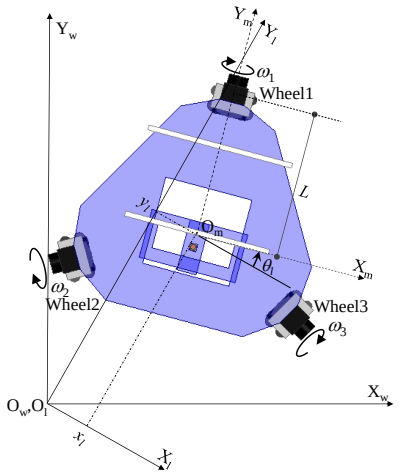

Figure 2. Kinematic model of ODV

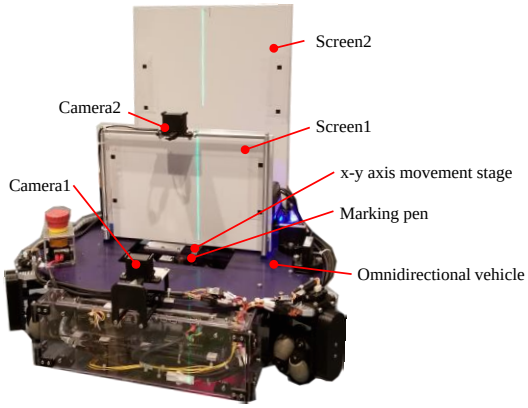

Figure 3. Photograph of marking robot

3 Composition of marking robot system

Our system consists of the MR and the LPU, each controlled by a computer. The two computers can communicate through the wireless network.

3.1 Marking robot (MR)

We use an omnidirectional vehicle (ODV) as the movement vehicle. It has three omnidirectional wheels mounted symmetrically, with 120 degrees between them. Each wheel is driven by a DC motor and is the same distance from the robot's center. Unlike the non-holonomic robots, this type of vehicle has a full mobility in the plane which means that at each instant it can move in any direction without any reorientation [9]. We can control the rotational speed of each wheel independently by sending commands to the motor driver. The kinematic model is shown in Figure 2. For the convenience of description, this paper defines three coordinate systems: Σ_w, the world coordinate system, Σ_R, the robot coordinate system, and Σ_L, the laser coordinate system, in which the coordinate Y_L axis corresponds to the direction of the line laser and the origin O_w and O_l are the same. Here ω_i (i=1,2,3) are the rotational velocities of the wheels (i represents the number of the wheel), R_w is the radius of the wheel, and L is the distance from the robot's center to the wheel. x_l, y_l, and θ_l are the positions and attitude angle in the Σ_L. The inverse-kinematic model in the Σ_L is represented in Equation (1) [10].

$$\begin{bmatrix}\omega_1\\ \omega_2\\ \omega_3\end{bmatrix} = \frac{1}{R_w}\begin{bmatrix}-\cos\theta_l & -\sin\theta_l & L\\ -\cos(\theta_l+2\pi/3) & -\sin(\theta_l+2\pi/3) & L\\ -\cos(\theta_l+4\pi/3) & -\sin(\theta_l+4\pi/3) & L\end{bmatrix}\begin{bmatrix}\dot{x}_l\\ \dot{y}_l\\ \dot{\theta}_l\end{bmatrix} \quad (1)$$

A photograph of the MR is shown in Figure 3. Two screens and cameras are placed on the ODV base. Screens 1 and 2 are parallel to each other and perpendicular to the floor. The distance between the screens is y_s. Cameras 1 and 2 face Screen 1 and 2 respectively and capture each screen image on which the laser spot and line are projected. The marking device is installed at the center of the robot. It consists of the x-y axis movement stage and the pen unit which can move the marking pen in the vertical direction. The pen unit can be moved on slider rails. By controlling the marking device, the cross mark is drawn on the floor.

3.2 Laser positioning unit (LPU)

This unit is composed of the guide laser unit (GLU) and the three dimensional measuring instrument (3D-MI: in our system, this is a Leica Geosystems 3D Disto. The accuracy of angle measurements is 5 seconds and the accuracy of the distance between two points about 10 m

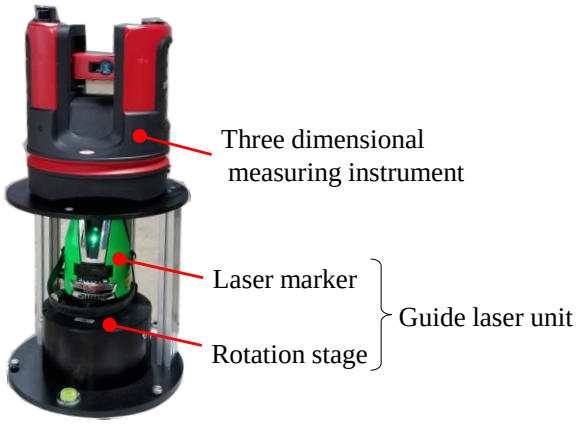

Figure 4. Photograph of laser positioning unit

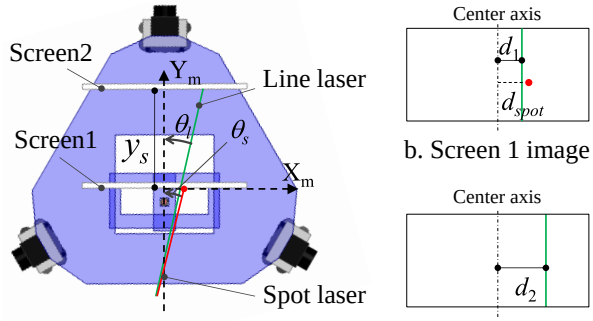

a. MR and laser layout b. Screen 1 image c. Screen 2 image

Figure 5. Screen layout and laser projected on the screen

apart is approximately 1 mm). Like a total station, the horizontal and vertical axes of the 3D-MI can be motorized. This can direct the point laser accurately in the direction indicated in advance and measure the distance to the object on which the laser spot is projected. The GLU consists of a laser marker and a rotation stage. The laser marker can generate a vertical line laser. Construction workers often use this for drawing a reference line on the floor, wall and ceiling and so on. This is placed on the rotation stage. The vertical axis of the 3D-MI agrees with that of the rotation stage. It is also motorized and the rotational speed is controlled through the RS485 interface. A photograph of the LPU is shown in Figure4.

4 Control of MR and LPU

4.1 Mechanism for measuring MR position

As shown in Figure 5, the attitude angle θ_l in the Σ_l is calculated from Equation (2), where, d_1 and d_2 are the x-coordinates of the laser line projected on each screen in the Σ_R. In the drawing cross mark phase, a laser spot is projected on Screen 1. Δx_r and Δy_r, which are respectively the movement values of the pen unit in the x and y-axis directions in the Σ_R are calculated from

Equation (3) and (4) using the geometric relationship, where, d_{spot} is the x-coordinate of the laser spot in the Σ_R, r_{screen} is the distance from the LPU to Screen 1, and θ_s is the attitude angle of the MR with respect to the direction of the spot laser. The laser spot does not necessarily overlap the laser line exactly because of the rotation stage control error. Since θ_l is nearly equal to θ_s, we use θ_l instead of θ_s in Equations (3) and (4). By controlling the marking device, the cross mark is drawn on the target position exactly.

$$\tan\theta_l = \frac{d_2 - d_1}{y_s} \quad (2)$$

$$\Delta x_r = d_{spot} + (r_{screen} - r_{tgt})sin\theta_s \quad (3)$$

$$\Delta y_r = (r_{screen} - r_{tgt})cos\theta_s \quad (4)$$

4.2 Detection of laser line and laser spot

It is difficult to measure the laser position accurately from a captured image without image processing because the captured image has two types of distortions which we have to remove. First, the lens distortion is removed by using Zhang's method [11]. Figures 6a and 6b show the screen images before and after the distortion removal. Subsequently, the perspective distortion is removed by the homography transformation, based on the following formulae:

$$\begin{cases} u_i = \dfrac{a + bs_i + ct_i}{1 + gs_i + ht_i} \\ v_i = \dfrac{d + es_i + ft_i}{1 + gs_i + ht_i} \end{cases} \quad (5)$$

Where

u_i,v_i: camera coordinates after the transformation

s_i,t_i: camera coordinates before the transformation

Eight unknown parameters a, b, c, d, e, f, g, h are obtained by solving the Equation (5) substituting a combination of more than four known points (u_i, v_i) and (s_i, t_i). In our system, a calibration mark is drawn on the screen. Four black squares are arranged at the four corners of a rectangle whose width and height are W and H respectively. Figures 6b and 6c show the screen images before and after the homography transformation. The position of the laser line and the laser spot are measured from this image. First, the red, green, and blue channels are extracted. In each channel image, the average pixel intensity of each column is calculated as shown in Figures 7a, 7b, and 7c. Since the laser marker emits a green laser in our system, the difference pixel intensity is calculated by subtracting half of the red and blue channel components from the green channel component as shown in Figure 7d. $u_{max,j}$ (j is the screen number) is the horizontal camera coordinate with the largest pixel intensity. d_j which is the x-coordinate of the laser line in the Σ_R is calculated using Equation (6).

$$d_j = (\frac{u_{max,j}}{N_H} - 1/2)W \quad (6)$$

Where, N_H is the number of the horizontal pixel.

The laser spot with the 3D-MI is red. A binarized image is obtained from a red channel image utilizing a binarization threshold. The binarized image is smoothed by expansion and contraction processing. As shown in Figure 8c, the laser line and block noise are removed and only the laser spot remains after this process. From this image, the area centroid is calculated. After that, as shown in Figure 8d, the masked image is obtained by setting the pixel intensity except for the 50 x 50 pixels square region centered on the area centroid to zero in the red channel image. The horizontal camera coordinate of the laser spot, $u_{max,spot}$, is calculated as the brightness center of gravity in this masked image. d_{spot} , which is the x-coordinate of the laser spot in the Σ_R, is also obtained from Equation (6). This image processing is conducted by the computer installed on the MR. The calculation cycle depends on the computer performance. In our system, it is approximately 0.17 seconds.

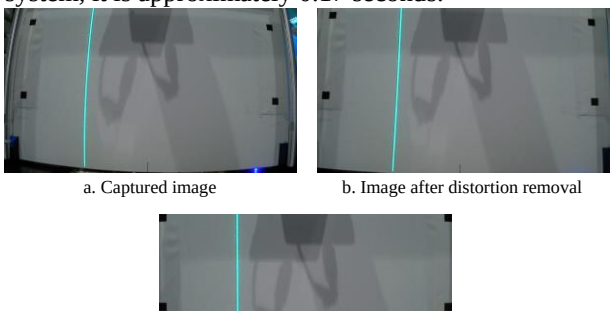

a. Captured image b. Image after distortion removal

c. Image after homography transformation

Figure 6. Images before and after distortion removal

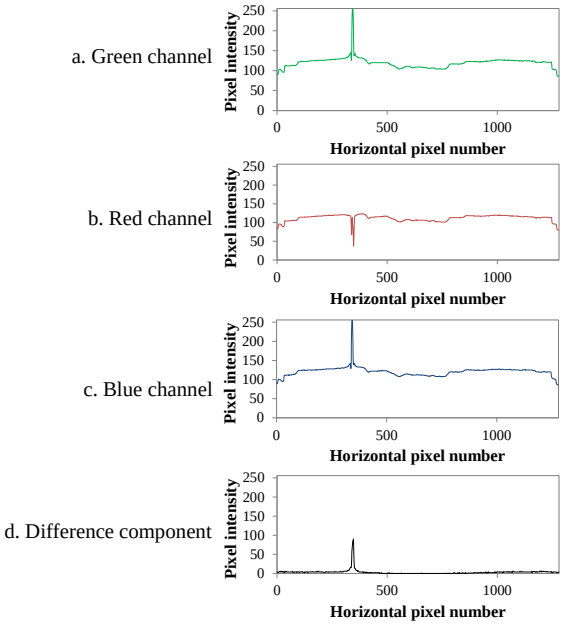

Figure 7. Average pixel intensity

a. Original image

b. Red channel image

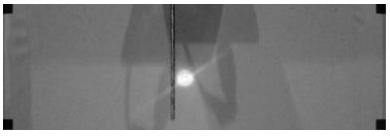

c. Binarized image

d. Masked image

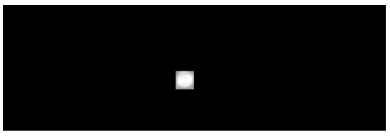

Figure 8. Spot laser image before and after image processing

4.3 Motion control

4.3.1 Control system

In our system, the MR tracks the line laser. The block diagram for tracking the line laser is shown in Figure 9. The meaning of each symbol is listed in Table 1. This PI (Proportional-Integral) control system feedback-controls the rotational speed based on the tracking error (e_x,e_θ) in Table 1. By converging the tracking error to zero, the MR tracks the laser line while keeping the screen perpendicular to the line laser. The actual center position and attitude angle is measured by the method detailed in the former section.

4.3.2 Traveling on the circular path

As explained in Section 2, as the line laser turns, the MR travels on circular path while keeping the screen perpendicular to the line laser. In the experimental setup shown in Figure 10, the tracking performance on the path was evaluated by changing the rotational speed of the rotation stage to 0.3, 0.6 and 0.9 degrees per second. The reference center position, attitude and translational velocity for the y axis direction in the Σ_l and the proportional and integral gains were set as listed in Table 2. Because $\dot{y}_{l,d}$ was set to zero, the MR tracked the moving line laser without approaching or moving away from the LPU. The proportional and integral gains were adjusted based on the values obtained in the simulation and preliminary experiment result. Figure 11 shows the relationship between x_l or θ_l and time. In the all rotational speed, the screen was nearly vertical to the

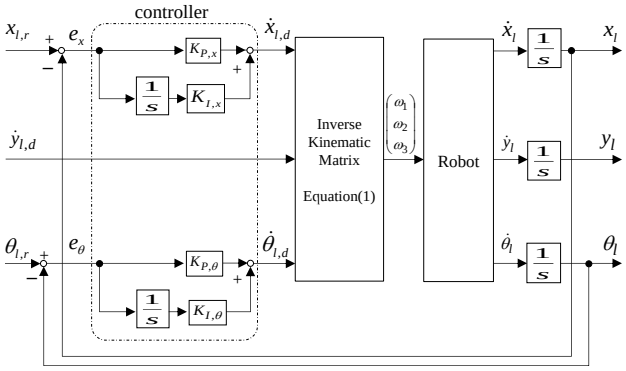

Figure 9. Control system

Table 1 Setting parameter

Parameters	Details
$(x_l,\ y_l,\ \theta_l)$	The actual coordinate and attitude of the MR in the Σ_l
$(x_{l,r},\ \theta_{l,r})$	The reference x-coordinate and attitude of the MR in the Σ_l
$(e_x,\ e_\theta)$	The deviation between the reference and actual value
$(\dot{x}_{l,d},\ \dot{y}_{l,d},\ \dot{\theta}_{l,d})$	The direction value of the translational and rotational speed of the MR in the Σ_l
$(\omega_1,\ \omega_2,\ \omega_3)$	The direction value of the rotational speed of each wheel
$(\dot{x}_l,\ \dot{y}_l,\ \dot{\theta}_l)$	The actual translational and rotational speed of the MR in the Σ_l
s	Differential operator

Table 2 Setting parameter

Parameter	value
$x_{l,r}$	0
$\theta_{l,r}$	0
$\dot{y}_{l,d}$	0
$K_{p,x}$, $K_{p,\theta}$, $K_{I,x}$, $K_{I,\theta}$	20, 0.244, 4, 0

line laser. When the screen is vertical to the line laser, x_l indicates the deviation between the line laser position and the screen center. In our system, W is 270mm. Although the laser line remained on the screen with any rotational speed, the translational speed of the laser line projected onto the screen increases as the distance between the MR and the LPU increases. Therefore, our system is designed to change the rotational speed of the rotation stage based on the distance from the LPU to the MR to prevent the laser line from being off the screen. That is, the rotational speed is inversely proportional to the distance.

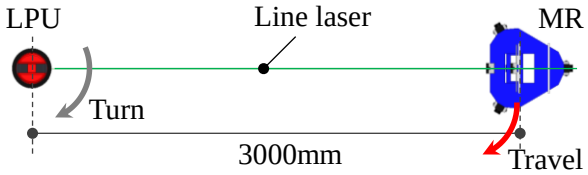

Figure 10. Experimental layout

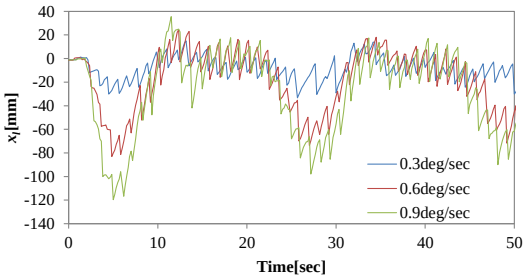

a. Relationship between x_l and time

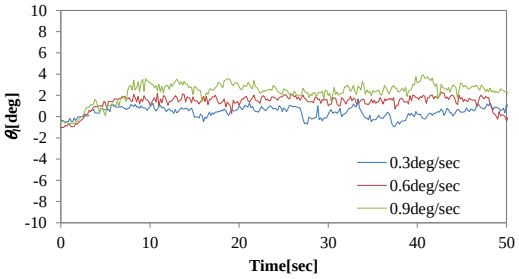

b. Relationship between θ_l and time

Figure 11. Tracking performance traveling on the circular path

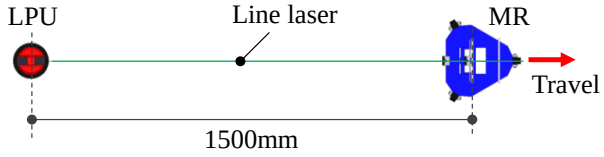

Figure 12. Experimental layout

4.3.3 Traveling on the straight line

When the line laser stops turning, the MR travels on the straight line connecting the LPU and the next target position while keeping the screen perpendicular to the line laser. In the experimental setup as shown in Figure 12, the tracking performance during travel on the straight line was evaluated. The setting parameters are listed in Table 3. Except for $\dot{y}_{l,d}$, they are the same as those for travel on a circular path. The MR travels at a speed of 50mm per second in the direction of the line. Figure 13 shows the relationship between x_l or θ_l and y_l. We confirmed that the MR stably traveled on the straight line until y_l was about 27 meters using this motion control method. The absolute values of x_l and θ_l were less than 25mm and 5 degrees respectively. Each standard deviation is 2.0mm and 0.5 degrees respectively. These values are very small.

Table 3 Setting parameter

Parameter	value
$x_{l,r}$	0
$\theta_{l,r}$	0
$\dot{y}_{l,d}$	50
$K_{p,x}$, $K_{p,\theta}$, $K_{I,x}$, $K_{I,\theta}$	20, 0.244, 4, 0,

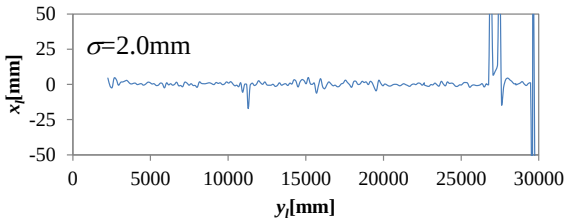

a. Relationship between x_l and y_l

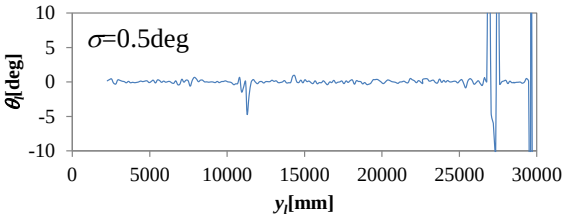

b. Relationship between θ_l and y_l

Figure 13. Tracking performance traveling on the straight line

5 Experiment

In order to evaluate the performance of the developed marking system, a basic test was executed. The experimental layout is shown in Figure 14. In the 4m x 10m test area, we set 50 target positions, which were grid intersections at intervals of 1m. The MR marked from Position A0 to Position J0 position in order. The total time spent marking was about 100 minutes. After marking all positions, the coordinates of the centers of every cross mark were measured using the 3D-MI.

Figure 15 shows the frequency distribution of x_l or θ_l, in the MR guidance phase. They are created from the measured x_l and θ_l every 0.17 seconds. They concentrate near zero. Each average value was 0.9mm and 0.03 degrees, and the standard deviation was 26.8mm and 1.2 degrees respectively. These results show that the MR stably tracked the line laser while controlling the attitude so that the laser line was in the screen center and vertical to the screen surface.

All of the deviations between the target positions and marked positions are summarized in Figure 16. Figure 16a shows the deviations at all marked positions. Figure 16b shows the deviations distribution. In this figure the radius of the red circle is 3mm. Figure 16c shows the frequency distribution of the deviation. The average deviation was 1.5mm, and the maximum value was 3.9mm. 94% of the measured values are within less than

3mm deviation. There is no strong correlation between the distance from the LPU to the MR and the deviation. Relatively large deviations are thought to be due to the local unevenness of the floor surface and detection error of the laser spot center from the screen image. By setting the target positions in advance, accurate and automatic marking was achieved in this system.

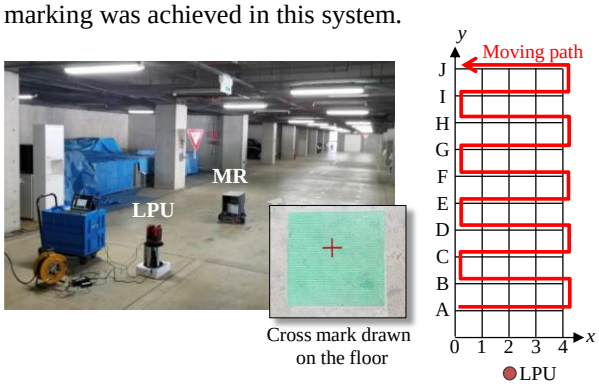

Figure 14. Experimental layout

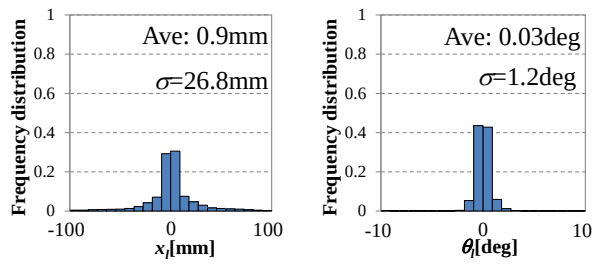

a. Frequency distribution of x_l b. Frequency distribution of θ_l

Figure 15. The performance for line laser tracking

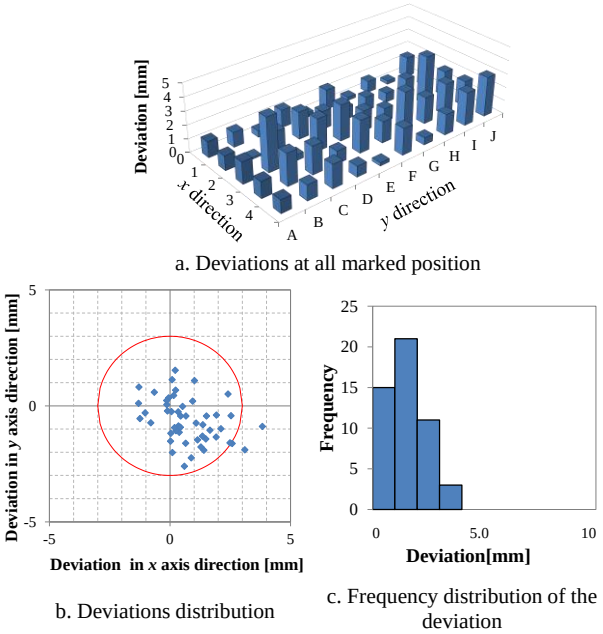

a. Deviations at all marked position

b. Deviations distribution

c. Frequency distribution of the deviation

Figure 16. Experimental Result

6 Conclusion and future research

We described the mechanism of our automated mobile marking system for free access floors in detail. In the experiment at the test site, the MR stably tracked the laser line generated by the LPU and then reached predetermined target positions. Furthermore, we confirmed the deviation between the mark drawn by the MR and the target coordinate was 1.5mm in average and 94% of the deviations are less than 3mm. This marking operation was fully automated. Therefore improved productivity in the construction work is expected.

However, some limitation can be identified. First, the time spent on marking is long. This work usually requires two workers using carpenter's ink pads or chalk line and measure. Experienced workers can mark with more than 10 times faster. Second, direct sunlight disturbs the detection of the line laser and the MR cannot track it. That is, the area where we can control the MR becomes smaller due to the influence of sunlight. Finally, some large deviations between the target positions and marked positions have been observed in the experiment. Some factors are considered. One is the local unevenness of the floor surface. The other is detection error of the laser spot center from the screen image. We have to solve these problems to improve performance of the MR in the future research.

Acknowledgement

The authors thank Dr. Eiji Koyanagi and Mr. Masayuki Miyashige from Mobile Robot Research Corporation LTD for their cooperation in the development of this mobile marking robot system.

References

[1] Shintaro Sakamoto, Hiroki Kishimoto, Kouetu Tanaka and Yukiteru Maeda. 3D Measuring and Marking System for Building Equipment: Developing and Evaluating Prototypes. *Proceedings of the 26th International Symposium on Automation and Robotics in Construction*, 131-138, Austin, USA, 2009

[2] Shintaro Sakamoto, Naruo Kano, Takeshi Igarashi, Hiroki Kishimoto, Hirohiko Fujii, Yuji Oosawa, Kentarou Minami and Kousei Ishida. Laser Marking System Based on 3D CAD Model. *Proceedings of the 28th International Symposium on Automation and Robotics in Construction*, 64-69, Seoul, Korea, 2011.

[3] Shintaro Sakamoto, Naruo Kano, Takeshi Igarashi, Hiroyuki Tomita. Laser Positioning System Using RFID-Tags. *Proceedings of the 29th International Symposium on Automation and Robotics in*

Construction, Eindhoven, The Netherlands, 2012.

[4] Kouetsu Tanaka, Makoto Kajitani, Chisato Kanamori, Hideki Itoh, Yasunori Abe and Yoshio Tanaka. Development of Marking Robot Working at Building Sites. *Proceedings of the 13th International Symposium on Automation and Robotics in Construction*, 235-242, Warsaw, Poland, 1996.

[5] Zulkifli Zainal Abidin, Syamsul Bahrin Abdul Hamid, Ahmad Anis Abdul Aziz and Azlan Ab Malek. Development of a Vision System for a Floor Marking Mobile Robot. *Proceedings of the 5th International Conference on Computer Graphics, Imaging and Visualization*, 88-92, Penang, Malaysia, 2008.

[6] Fumihiro Inoue, Satoru Doi and Eri Omoto. Development of High Accuracy Position Making System Applying Mark Robot in Construction Site. *SICE Annual Conference 2011*, 2413-2414, Tokyo, Japan, 2011.

[7] Fumihiro Inoue and Eri Omoto. Development of High Accuracy Position Marking System in Construction Site Applying Automated Mark Robot. *SICE Annual Conference 2012*, 819-823, Akita, Japan, 2012.

[8] DPR construction, 'Laybot Shows Promise in Speed and Accuracy', 2013 [Online]. Available: https://www.dpr.com/media/news/2013 [Accessed: 22- Feb- 2018]

[9] Guy Campion, Georges Bastin and Brigitte D' Andrea-Novel. Structural Properties and Classification of Kinematic and Dynamic Models of Wheeled Mobile Robots. *IEEE Transactions on Robotics and Automation*, 12(1), 47 -62, 1996.

[10] Hsu-Chih Huang, Ter-Feng Wu, Chun-Hao Yu and Huan-Shiuan Hsu. Intelligent Fuzzy Motion Control of Three-Wheeled Omnidirectional Mobile Robots for Trajectory Tracking and Stabilization, *Proceedings of 2012 International Conference on Fuzzy Theory and Its Applications*, 107-112, Taichung, Taiwan.

[11] Z. Zhang. A flexible new technique for camera calibration. *IEEE Transactions on Pattern Analysis and Machine Intelligence*, 22(11), 1330-1334, 2000.